Retinoblastoma Is Characterized by a Cold, CD8+ Cell Poor, PD-L1− Microenvironment, Which Turns Into Hot, CD8+ Cell Rich, PD-L1+ After Chemotherapy

Clelia Miracco,[1] Paolo Toti,[1] Maria Chiara Gelmi,[2] Sara Aversa,[1] Gennaro Baldino,[3] Paolo Galluzzi,[4] Sonia De Francesco,[2] Federica Petrelli,[1] Ester Sorrentino,[1] Giuseppe Belmonte,[1] Daniela Galimberti,[5] Sandra Bracco,[6] and Theodora Hadjistilianou[2]

[1]Department of Medicine, Surgery and Neuroscience, Pathological Anatomy Section, University Hospital of Siena, Siena, Italy
[2]Department of Medicine, Surgery and Neuroscience, Ophthalmology Unit, University Hospital of Siena, Siena, Italy
[3]Department of Health Promotion Sciences, Maternal and Infant Care, Internal Medicine and Medical Specialties (PROMISE), University of Palermo, Palermo, Italy
[4]Department of Medicine, Surgery and Neuroscience, Unit of Neuroimaging and Neurointervention, University Hospital of Siena, Siena, Italy
[5]Department of Maternal, Newborn and Child Health, Unit of Pediatrics, University Hospital of Siena, Siena, Italy
[6]Department of Medicine, Surgery and Neuroscience, Unit of Neuroimaging and Neurointervention, University Hospital of Siena, Siena, Italy

Correspondence: Maria Chiara Gelmi, Department of Medicine, Surgery and Neuroscience, Ophthalmology Unit, University Hospital of Siena, Siena, Italy; mariachiara.gelmi@student.unisi.it.

Received: August 5, 2020
Accepted: January 3, 2021
Published: February 4, 2021

Citation: Miracco C, Toti P, Gelmi MC, et al. Retinoblastoma is characterized by a cold, CD8+ cell poor, PD-L1− microenvironment, which turns into hot, CD8+ cell rich, PD-L1+ after chemotherapy. *Invest Ophthalmol Vis Sci.* 2021;62(2):6. https://doi.org/10.1167/iovs.62.2.6

Purpose. To investigate the impact of chemotherapy (CHT) on human retinoblastoma (RB) tumor microenvironment (TME).

Cases and Methods. Ninety-four RBs were studied, including 44 primary RBs treated by upfront surgery (Group 1) and 50 primary RBs enucleated after CHT (CHT), either intra-arterial (IAC; Group 2, 33 cases) or systemic (S-CHT; Group 3, 17 cases). Conventional and multiplexed immunohistochemistry were performed to make quantitative comparisons among the three groups, for the following parameters: tumor-infiltrating inflammatory cells (TI-ICs); programmed cell death protein 1 (PD-1) positive TI-ICs; Ki67 proliferation index; gliosis; PD-1 ligand (PD-L1) protein expression; vessel number. We also correlated these TME factors with the presence of histological high-risk factors (HHRF+) and RB anaplasia grade (AG).

Results. After CHT, a decrease in both RB burden and Ki67 positivity was observed. In parallel, most subsets of TI-ICs, PD-1+ TI-ICs, gliosis, and PD-L1 protein expression significantly increased ($P < 0.001$, $P = 0.02$, $P < 0.001$, respectively). Vessel number did not significantly vary. Age, HHRFs+ and AG were significantly different between primary and chemoreduced RBs ($P < 0.001$, $P = 0.006$, $P = 0.001$, respectively) and were correlated with most TME factors.

Conclusions. CHT modulates host antitumor immunity by reorienting the RB TME from anergic into an active, CD8+, PD-L1+ hot state. Furthermore, some clinicopathological characteristics of RB correlate with several factors of TME. Our study adds data in favor of the possibility of a new therapeutic scenario in human RB.

Keywords: retinoblastoma, tumor microenvironment, chemotherapy, PD-1/PD-L1, multiplexed immunohistochemistry

Therapy increased retinoblastoma (RB) survival up to over 95%, with a high rate of eye salvage in high-income countries.[1,2] There is an array of therapy approaches, ranging from upfront surgery to local treatments.[1] Chemotherapy (CHT) alone or coupled with other treatments is now the preferred conservative approach.[1] Despite therapy, a number of RBs progress, prompting the search for new approaches.[3]

The study of tumor microenvironment (TME) has been providing knowledge for novel therapies in cancer.[4] TME consists of a mix of cancerous and noncancerous components and their products, which play complex, bidirectional, immunostimulant, and immunosuppressive interactions, from which the immune response against cancer derives.[4]

A mechanism to escape the immune response in cancer is the activation of negative regulatory pathways (immune checkpoints [i-CPs]), which, under normal physiological conditions, maintain immune homeostasis.[5] Interactions between suppressive i-CPs and their ligands inhibit the

response of effector immune cells, usually by inducing T-cell exhaustion, with a progressive loss of effector functions, and coexpression of inhibitory receptors.[5] Both cancer cells and nontumor cells may overexpress i-CPs, thus limiting normal antitumor immune responses.[5] The blockade of i-CPs is a novel immunotherapeutic approach to potentiate host immunological responses against neoplasms, already used for a number of cancers.[5] Two members of the B7 family are among the most widely investigated i-CPs: programmed cell death receptor-1 (PD-1) and programmed cell death ligand-1 (PD-L1); PD-L1 inhibitors are already used for cancer therapy.[5]

The effectiveness of i-CP blockade largely depends on the presence of inflammatory/immune cells within the tumor tissue and on the expression of the targeted i-CP by TME.[6] Nowadays, the frequency of tumor-infiltrating lymphocytes and the expression levels of PD-L1 in cancer tissue are used as prognostic markers and as predictors of response to PD-L1/PD-1 inhibitor therapy in several cancer types.[6,7]

The TME of RB is still sparsely explored.[8–20] There are only few investigations on the impact of CHT on RB TME.[16–20]

In the present study, in a cohort of 94 patients who underwent enucleation for RB, we investigated the following elements at the tumor tissue level: the frequency of several subsets of TI-ICs, including lymphocytes, dendritic-like cells, macrophages and myeloid-derived suppressor-like granulocytic (G-MDS-like) cells, the RB proliferation rate, the extent of gliosis, the protein expression of PD-L1 and PD-1, and the number of vessels. Investigations were conducted by conventional and multiplexed immunohistochemistry. The latter allows the simultaneous detection of multiple TME antigens in tumor tissues[21] and was validated by immunofluorescence.

The presence of histological high-risk factors (HHRFs) according to the International RB Staging Working Group guidelines[22] and the degree of anaplasia according to Mendoza et al.[23] (AG-M) were also assessed. Data were compared among RBs subdivided into three groups: group 1 (44 cases), with no previous treatment; group 2 (33 cases), treated with local CHT (IAC); and group 3 (17 cases), treated with systemic CHT (S-CHT) before enucleation.

Methods

Case Series (Patients, Samples and Research Ethics)

Archival, formalin-fixed, paraffin-embedded tissue samples from 143 consecutive RBs of 133 patients operated on for RB from 2010 to 2019 at the Ophthalmology Unit of the University Hospital of Siena were retrieved. Exclusion criteria were previous radiotherapy or treatments at other Institutions and tumor tissue not sufficient to perform our analyses or altered by severe vascular complications

The final case study consisted of 94 cases, which included 44 patients without any prior therapy (group 1), and 50 patients who underwent chemotherapy before enucleation,[24] alone or combined with other treatments, subdivided into 33 patients treated with IAC (group 2) and 17 patients treated with S-CHT (group 3). In all cases, written informed consent was obtained from parents or caregivers. The median follow-up in months was 50 (range 12–99), 67 (range 13–116), and 73 (range 14–115) for groups 1, 2, and 3, respectively. In 23 of 24 cases of bilateral RB, one eye was not investigated, because it met the exclusion criteria. The study was approved by the local Ethical Committee and carried out according to the Declaration of Helsinki (revised 2013, World Medical Association).

Histopathological Procedures

For each tumor, histology was reassessed on hematoxylin and eosin-stained slides by two pathologists (C.M., P.T.) blinded to clinical data, according to the latest American Joint Committee on Cancer 2018 pathologic classification and staging system.[25] Tumor pT and the following features were reviewed: growth pattern (endophytic, exophytic, mixed, diffuse); histological grade (well, moderately, or poorly differentiated); tumor seeding (vitreous, subretinal). The degree of anaplasia was also assessed in each case according to Mendoza et al.[25] (AG-M): 1 (retinocytoma), 2 (mild anaplasia), 3 (moderate anaplasia), and 4 (severe anaplasia); the highest AG-M registered that occupied >10% of the tumor was assigned in each case. The presence of the following histological high-risk factors (HHFR) was also registered, according to the International Retinoblastoma Working Group: postlaminar optic nerve (ON) invasion, massive choroidal invasion, prelaminar or laminar ON invasion combined with nonmassive choroidal invasion, RB invasion of the anterior segment, extraocular diffusion.[22]

In each case, the TME parameters to be studied were evaluated on immunostained sections.

Conventional Immunohistochemistry

Immunohistochemistry was performed as previously described,[26,27]using the Ventana Benchmark ULTRA automatic devices (Ventana; Roche Diagnostics, Monza, Italy). For each case, we examined two to three tissue blocks, including standard pupil–optic nerve sections. Briefly, 3 μm–thick serial sections were deparaffinized, rehydrated and incubated at 37°C with the primary antibodies (listed in Table 1), according to manufacturers' instructions. Subsequently, the appropriate secondary antibody was applied, and the sections were counterstained with Hematoxylin II (Ventana). We applied the UltraView Universal Detection kit (Ventana), using HRP multimer and either diaminobenzidine or new fuchsin as chromogens. Each reaction was run with appropriate positive and negative controls; for the latter the primary antibodies were omitted.

Multiplexed Immunohistochemistry

Multiplexed immunohistochemistry was performed on the platform Ventana Discovery by applying the recommended protocol. The multiple immunostains performed are shown in Table 2.

Immunofluorescence

To validate multiplexed immunohistochemistry, immunofluorescence was carried out in representative cases of each group, as previously described.[28]

Quantitative Evaluation of Immunostaining

Five to 15 high-power fields (HPF) were evaluated at magnification × 400 (one HPF = 0.16 mm^2), avoiding necrotic

Investigative Ophthalmology & Visual Science

Table 1. Targets, Targeted Antigens (Ag), and Characteristics of Antibodies (Ab) Used in This Study

Target	Ag	Ab-Clone	Species	Source	Dilution
T helper lymphocytes	CD4	SP35	Rabbit	Ventana	Ready to use
T cytotoxic lymphocytes	CD8	SP57	Rabbit	Ventana	Ready to use
Cytotoxic granules	Granzyme b	11F1	Rabbit	Ventana	1:50
Cytotoxic granules	TIA-1	2G9A10F5	Mouse	Biogenex	1:50
B lymphocytes	CD20	L26	Mouse	Ventana	Ready to use
Regulatory T cells	FOXP3	mAbcam22510	Mouse	ABCAM	1:50
Dendritic-like cells	CD1a	EP3622	Rabbit	Ventana	Ready to use
Macrophages	CD68	KP1	Mouse	Ventana	Ready to use
M2 macrophages	CD163	10D6	Mouse	Novocastra	Ready to use
TI-ICs-RB cells	PD-1	NAT105	Mouse	Ventana	Ready to use
Glial cells	GFAP	EP672Y	Rabbit	Ventana	Ready to use
TI-ICs-RB cells	PD-L1	SP263;CD274/B7H1	Rabbit; mouse	Ventana; LsBio	Ready to use
RB cell nuclei proliferation antigen	Ki67	30/09/20	Rabbit	Ventana	Ready to use
Dendritic-like cells	S100	Polyclonal	Rabbit	Ventana	Ready to use
G-MDS-Like cells	CD15	MMA	Mouse	Ventana	Ready to use
RB cells	Synaptophysin	SP11	Rabbit	Ventana	Ready to use
MDS-like cells	CD11b	Polyclonal	Rat	Invitrogen	1:50
MDS-like cells	CD14	Polyclonal	Rabbit	Invitrogen	1:50
Endothelium of vessels	CD34	QBEnd/10	Mouse	Ventana	Ready to use

Table 2. Aims, Targeted Cells and Multiplexed Immunostaining Performed in This Study

Aim And Targeted Cells	Multiple Immunostains
To identify CD4+ macrophages to be differentiated from CD4+ lymphocytes	CD4/CD68
To identify dendritic-like cells	CD1a/S100
To identify G-MDS-like cells	CD11b/CD14/CD15
To co-localize cytotoxic TIA1+ granules and PD-1 within CD8+ lymphocytes	CD8/TIA-1/PD-1
To co-localize cytotoxic TIA1+ granules and PD-L1 within CD8+ lymphocytes	CD8/TIA-1/PD-L1
To co-localize PD-L1 within either CD68+ macrophages or glial cells	CD68/GFAP/PD-L1
To co-localize PD-L1 within either CD163+ macrophages or glial cells	CD163/GFAP/PD-L1
To co-localize PD-1 either in RB cells or in CD8+ lymphocytes	Synaptophysin/CD8/PD-1
To co-localize PD-L1 either in RB cells or in CD8+ lymphocytes	Synaptophysin/CD8/PD-L1

and calcified areas. In some group 2 and 3 cases, five fields covered the entire lesional area. Immunopositivity was manually assessed through computer-assisted stereology. Briefly, TIFF images (resolution: 1160 × 835 pixels) were captured from each field by an optical system composed of a Zeiss Axiocam MRc5 mounted on a Zeiss Axioscope 40 microscope (AxioVision Rel. 4.41 software version; Zeiss, Oberkochen, Germany) and analyzed through the public domain ImageJ processing tool (imagej.nih.gov/ij; ImageJ software, version 1.50i).

Immunostained TI-ICs and PD-1+ TI-ICs were counted at random, starting from areas with the highest density ("hot spot" areas). The proliferation index (PI) was the percentage of Ki67 positive nuclei, on all nuclei. GFAP+ areas were assessed as the percentage in the entire lesion. All PD-L1 positivity (PD-L1+tumor areas and PD-L1+ TI-ICs) was measured in each field according to literature recommendations[29] and expressed as the percentage in the lesional area.

CD34 labeled vessels were counted in each HPF.

Statistics

The statistical analyses were carried out using IBM SPSS 25. First, Shapiro Wilk test was used to check whether the data were normally distributed, both in the total cohort and when dividing the cases by treatment group. Next, we compared the histopathological features in the three groups (group 1: no CHT, group 2: IAC, and group 3: S-CHT). We used the Kruskal Wallis test to compare continuous variables across the three groups. Spearman's correlation coefficient was used to study the correlation between clinicopathological variables and TME components. We tested the correlation between TME components and the single HHFs with Kruskal-Wallis test.

Results

Clinicopathological Features

The main clinicopathological data of the final cohort of 94 RBs are shown in Table 3.

Group 1 (Primary RBs; $n = 44$)

Pathological stage was pT3 to pT4 in 59.1% of the cases. International Classification of Retinoblastoma (ICRB) groups D and E constituted 81.8% of the cases. At histology, most cases showed a diffuse proliferation of small blue cells, with frequent mitoses, admixed to necrosis and calcifications, without or with occasional Homer Wright or Flexner-Wintersteiner rosettes. Large, hyperchromatic, and pleomorphic nuclei were also observed in a number of cases. In two eyes, retinocytoma-like areas were seen.

A high (G3-G4) histological grade and a high (3-4) anaplasia grade were assigned to 77.3% and 63.6% of cases, respectively. One or more HHRFs were found in 28 (63.6%) cases.

Investigative Ophthalmology & Visual Science

Table 3. Demographic Information and Main Clinicopathological Features at Diagnosis of Patients in Group 1 (No Treatment Before Enucleation), 2 (IAC) and 3 (S-CHT) With or Without Additional Therapies*

	Group 1	Group 2	Group 3
Number of patients	44	33	17
Gender (M:F)	18:26	18:15	10:7
Age in months median (range)	29 (1–66)	46, 38 (14–136)	38, 53 (4–142)
Follow-up in months median (range)	50 (12–99)	67 (13–116)	73 (14–115)
Laterality (U:B)	37:7	30:3	3:14
pT†	pT1: 9; pT2a: 9; pT3a: 8; pT3b: 6; pT3c: 3; pT4: 9.	pT1: 20; pT2a: 6; pT2b: 2; pT3a: 4; pT3c: 0; pT4: 1.	pT1: 8; pT2a: 4; pT3a: 5
ICRB Grouping‡	B: 1; D: 6; E: 30; NA: 7	B: 5; C: 5; D: 15; E: 4; NA: 4	B: 2; C: 2; D: 6; E: 4; NA: 3
IViC	None	10	None
Laser	None	6	5
Criotherapy	None	12	None
IAC	None	33	11
Reason for enucleation	ED (34); Gl (9); UN (3)	DP (18); DPr (9); PhB (4); Gl (2)	DP (7); DPr (6); PhB (2); Gl (1); Vl (1)
Growth pattern	End (20; 45.45%); Ex (6; 13.33%); Mix (18; 40.91%); Din: 1 (2.27%)	End (21; 63.64%); Ex (2; 6.06%); Mix (10; 30.3%)	End (14; 82.35%); Ex (2; 11.76%); Mix (1; 5.88%)
Histological Grade (1–4)†	1 (2; 4.54%); 2 (8; 18.18%); 3 (28; 63.63%); 4 (6; 13.63%)	1 (11; 33.33%); 2 (6; 18.18%); 3 (16; 48.48%)	1 (5; 29.41%); 2 (3; 17.65%); 3 (9; 52.94%)
Retinocytoma Areas	2 (4.54%)	11 (33.33%)	5 (29.41%)
Seeding	Vi (19; 43.18%); Sr (12; 27.27%)	Vi (11; 33.33%); Sr (4; 12.2%)	Vi (4; 23.53%); Sr (2; 11.76%)
AG-M (1–4)	2 (16;36.36%); 3 (23; 52.27%); 4 (5; 11.36%)	1 (2; 6.06%); 2 (24; 72.73%); 3 (7; 21.21%)	2 (11; 64.71%); 3 (6; 35.29%)
HHRFs‡	*n*, 28 (63.6%) Pl-Oni (13;29.55%); mCHi (14; 31.82%); ASi (10;22.73%); ExO (5; 11.36%)	*n*, 9 (27.3%) Pl-ONi (1; 3.03%); mCHi (8; 24.24%); ASi (4; 12.12%)	*n*, 7 (41.2%) Pl-ONi (1; 5.88%); mCHi (5; 29.41%); ASi (3; 17.65%)

ED, extension of disease; Gl, glaucoma; UN, unknown; DP, persistence of disease; DPr, progression of disease; PhB, phthisis bulbi; vL, visual loss; End, endophytic; Ex, exophytic; Mix, mixed; Din, diffuse infiltrating; Vi, vitreal; Sr, subretinal; AG-M, anaplastic grade according to Mendoza et al.[23] ; Pl-Oni, postlaminar optic nerve invasion; mCHi, massive choroidal invasion; ASi, invasion of anterior segment; ExO, extraocular diffusion; NA, not available; IviC, intravitreal chemotherapy.

* As previously described,[24] IAC consisted in three monthly sessions with 5 mg/kg melphalan, and S-CHT was based on VEC protocol, which included vincristine 0.05 mg/kg, ethoposide 5 mg/kg, and carboplatin 25 mg/kg, administered in six sessions at four-week intervals.

† American Joint Committee on Cancer 2018.[25]

‡ Determined at diagnosis according to the ICRB.[22]

Two patients died; in both cases, RB infiltrated the transected end of the optic nerve, leading to extraocular tumor spreading.

Group 2 (IAC Chemoreduced RBs; *n* = 33)

Pathological stage was pT3-4 in 15.15 % of the cases. ICRB groups D and E constituted 57.6% of the cases. In most cases, gliotic areas and calcifications largely replaced RB tissue, in which rosettes were variably found. Retinocytoma-like areas were observed in 11 cases (33.3%); in two of which RB was virtually absent. Highly pleiomorphic RB areas were not observed. A high (G3) histological grade and a high (3) anaplasia grade were assigned to 48.5% and 21.2% of cases, respectively. One or more HHRFs were found in nine (27 .3%) cases. At the last follow-up, no patients died of the disease

Group 3 (S-CHT Chemoreduced RBs; *n* = 17)

Pathological stage was pT3 in 29.4% of the cases. ICRB groups D and E constituted 56.8% of the cases. All cases showed gliosis, calcifications, and viable retinoblastoma tissue, variably forming rosettes. Retinocytoma-like areas were detected in five cases (29.4%). There were no highly pleiomorphic RB areas. A high (G3) histological grade and a high (3) anaplasia grade were assigned to 52.9% and 35.3% of cases, respectively. One or more HHRFs were found in seven (41.2%) cases. At the last follow-up, no patients died of the disease

Retinoblastoma Microenvironment Features

In group 1, in most cases, all TI-ICs subsets were sparse and found in perivascular region and nearby necrotic areas (Figs. 1A, 1B, 1G). Most of them were macrophages. Ki67 labeled a high number of viable RB cells. In retinocytoma-like areas, a low frequency of KI67+ nuclei was observed. In the normal retina, PD-L1 positivity was mostly found in the retinal pigmented epithelium and in GFAP+ glial cells (Fig. 2). Perivascular and intratumoral GFAP+ glial cells also expressed PD-L1 (Figs. 2 and 3). Few RB cells near necrotic areas showed PD-L1 positivity (Figs. 4A, 4B). PD-L1+ and PD-1+ TI-ICs were very rare. In the normal retina, PD-1 positivity was seen mainly within the ganglion cell layer. Both PD-L1 and PD-1(Fig. 5C) positivity increased in retinal areas closest to RB. In 9 cases (20.5%), a patchy, weak-to-moderate-to-strong PD-1 immunopositivity was observed in RB cells (Fig. 5C-D). In five cases, TI-ICs were easily observed, mostly within large GFAP+, PD-L1+ gliotic areas,

Investigative Ophthalmology & Visual Science

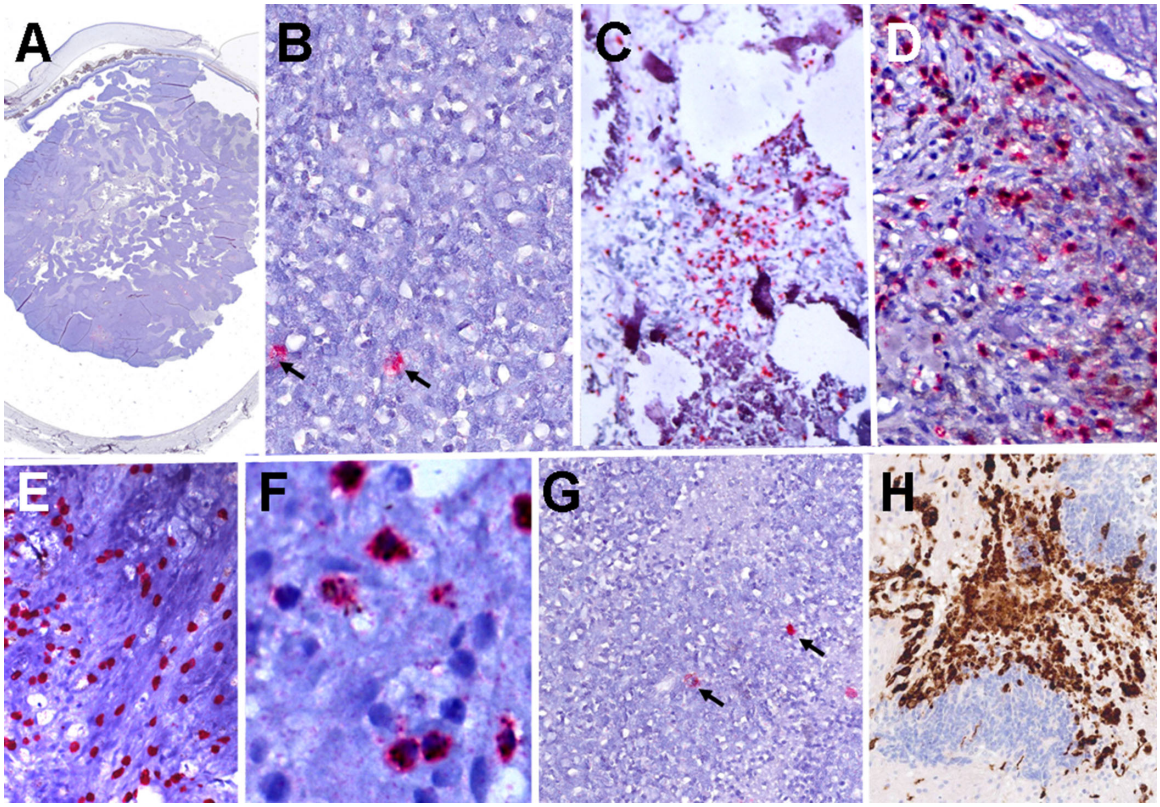

Figure 1. Conventional immunohistochemistry for CD8 (**A–D**); TIA-1 (**E, F**) and CD163 (**G, H**). (**A, B**) A representative case of group 1 showing very few CD8+ lymphocytes (**B**, *arrows*). (**C, D**) A group 2 (**C**) and a group 3 (**D**) RB showing CD8+ lymphocyte high density withing a gliotic area. (**E, F**) TIA-1–positive lymphocytes in another group 3 RB; granular cytoplasmic TIA-1 positivity is appreciable at a higher magnification (**F**). (**G, H**) A group 1 RB, showing rare CD163-positive macrophages (**G**, *arrows*). High number of CD163-positive macrophages in a group 3 case (**H**). Magnification: **A**: ×1; **B, D, E, G, H**: ×200; **C**, ×100; **F**, ×400. (**A–G**) The red chromogen new fuchsin was used. (**H**) The brown chromogen diaminobenzidine was used.

partly merging with retinocytoma-like areas. In these cases, KI67 positivity was low.

CD34 stained the endothelium of thin-walled, regularly shaped vessels, usually surrounded by aggregates of viable RB cells.

In group 2, in 32 cases (96.96%), heterogeneously distributed TI-ICs were easily found, most frequently in gliotic areas (Fig. 1C). CD8+ lymphocytes usually coexpressed TIA-1 (Figs. 5A, 5B). PD-L1 colocalized with GFAP in glial cells (Figs. 6A–6E). TI-ICs were also found admixed with RB cells. One case had large areas of viable RB cells, few TI-ICs, and high KI67 proliferative index and showed limited GFAP+ and PD-L1+ areas. In eight cases (24.2%), a patchy, weak-to moderate-to strong PD-1 immunopositivity was observed in RB cells (Figs. 5A, 5B).

In group 3, there were numerous heterogeneously distributed TI-ICs (Figs. 1D, 1E, 1F, 1H), mainly in gliotic areas and mixed with RB cells. Coexpression of GFAP and PD-L1 was observed (Figs. 6F–6J). Three cases (17.6%) showed a heterogeneous, patchy, weak-to moderate-to strong immunopositivity to PD-1 in RB cells (Figs. 5E, 5F).

TI-ICs were also observed in normal ocular structures in all chemoreduced RBs, mainly within the choroid.

In both groups 2 and 3, Ki67 positivity was heterogeneous, high in RB viable cells, and low in retinocytoma-like areas and in gliotic areas (Figs. 4C, 4D). In both groups 2 and 3, CD34-positive, thin-walled, regularly-shaped vessels were observed within RB tissue and gliotic areas.

In all groups, no coexpression of CD8 and PD-1 was found,

Statistics

The median and range of values for each parameter are reported in Table 4. Data were not normally distributed (see Supplementary Tables S1 and S2); therefore we used nonparametric testing for the subsequent analyses.

As shown in Table 4, patient age was significantly ($P < 0.0001$) lower in group 1 than in group 2 but there was no significant difference between groups 1 and 3 nor between groups 2 and 3. The number of cells expressing CD4, CD8, granzyme B, TIA-1, CD1a/S100, CD68 and CD163 was significantly ($P < 0.0001$) higher in group 2 and group 3 cases compared to group 1 cases, as were GFAP and PDL1 positivity, but there was no significant difference between the two groups that received chemotherapy (groups 2 and 3). The proliferation index Ki67, on the contrary, was significantly ($P < 0.0001$) higher in group 1 than in groups 2 and 3. The number of PD1+ cells was significantly ($P = 0.04$) higher in group 2 compared to group 1, but there was no significant difference between groups 1 and 3 nor between groups 2 and 3. CD11b+/CD14-/CD15+ cells were significantly ($P = 0.001$) less in group 2 compared to group 1, but no significant difference was found between groups 1 and 3 nor between groups 2 and 3. The number of cells expressing CD20 and FOXP3 and the number of CD34+ vessels did not

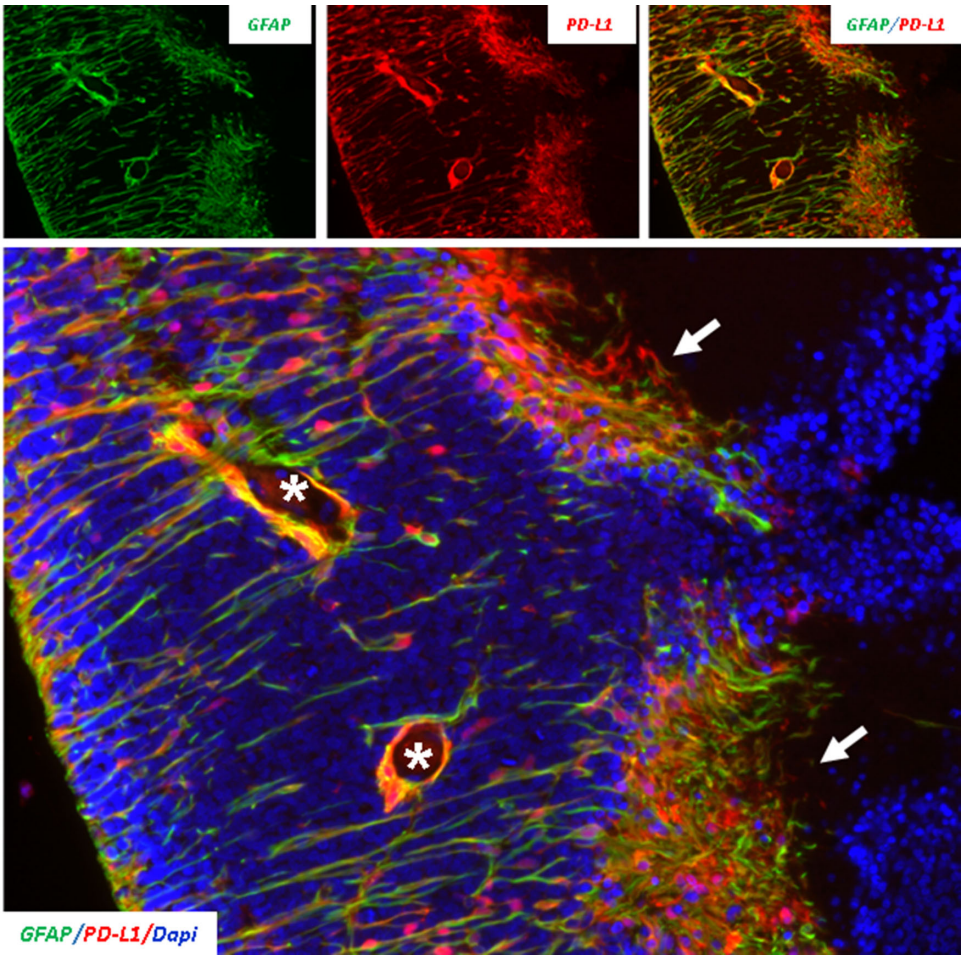

Figure 2. GFAP (*green*) and PD-L1 (*red*) double immunofluorescence in a group 1 RB showing regression. Nuclei are stained blue with DAPI. GFAP (*green*) and PDL1 (*red*) positivity colocalize within a gliotic area (*arrows*). Perivascular glial cells (*asterisks* in the vessel lumen) and glial cells in the retina show colocalization of GFAP and PD-L1 as well. Nuclei (*blue*) of PD-L1-negative viable RB cells are recognizable within the gliotic area (*arrows*) and infiltrating the retina. Merge images in the box at the top (GFAP and PD-L1), on the *right* and in the *bottom box* (GFAP, PD-L1, and DAPI). Magnification × 200. Immunofluorescence: Fluorescein isothiocyanate, *green*; Rhodamine, *red*; DAPI, blue secondary fluorochrome–conjugated antibody (goat anti-rabbit Alexa Fluor 488 [*green*], goat anti-mouse Alexa Fluor 568 [*red*]).

show any significant difference among the groups. Figure 7 shows the distribution of the parameters across the three groups.

When considering clinicopathological factors, group 1 cases more frequently had HHRFs and a higher AG-M than group 2 and group 3 cases (Table 5).

The presence of HHRFs (Table 6) is directly correlated with CD11b+/CD14−/CD15+ ($P = 0.007$) and Ki67 ($P = 0.004$), that were higher in group 1, whereas it was inversely correlated with CD8+ ($P = 0.03$), granzyme B+ ($P = 0.04$), TIA-1+ (0.03), GFAP% ($P = 0.008$) and PD-L1% (0.01), that were lower in group 1. Similarly, a higher AG-M was directly correlated with FOXP3+ ($P < 0.001$), CD11b+/CD14−/CD15+ ($P = 0.03$), and Ki67% ($P < 0.001$), whereas it was inversely correlated with CD4+ ($P = 0.02$), CD8+ ($P < 0.001$), granzyme B+ ($P < 0.001$), TIA-1+ ($P < 0.001$), CD1a+/S100+ ($P < 0.001$), CD68+ ($P < 0.001$), CD163+ ($P < 0.001$), GFAP% ($P < 0.001$), PD-1+ ($P = 0.03$), and PD-L1% ($P < 0.001$). Considering the HHRFs individually, none of them showed a statistically significant correlation with TME factors (data not shown).

Discussion

Chemotherapy induces RB regression, and RBs may rarely regress spontaneously as well. Ophthalmoscopy and imaging give a reliable estimate of the histopathology and degree of regression.[30–37] Upon regression, RB becomes smaller and shows calcifications. Changes in the TME of regressed RB are largely unknown.

In untreated RBs (group 1), we appreciated very few TI-ICs in most cases. Conversely, a large number of TI-ICs was observed in 49 of 50 chemoreduced RBs and in five group 1 cases that showed spontaneous regression.

The immune response and the number of TI-ICs within a tumor largely depend on its immunogenicity,[4] RB is a poorly immunogenic neoplasm, which may justify its low frequency of TI-ICs.[8,38] Immunogenicity is also associated with response to i-CP blockade.[39] Immunologically "hot/inflamed," "warm," and "cold/non-inflamed" tumor histologic specimens based on tumor-infiltrating lymphocyte density and PD-L1 expression have been correlated to different therapy responses.[6,7]

Investigative Ophthalmology & Visual Science

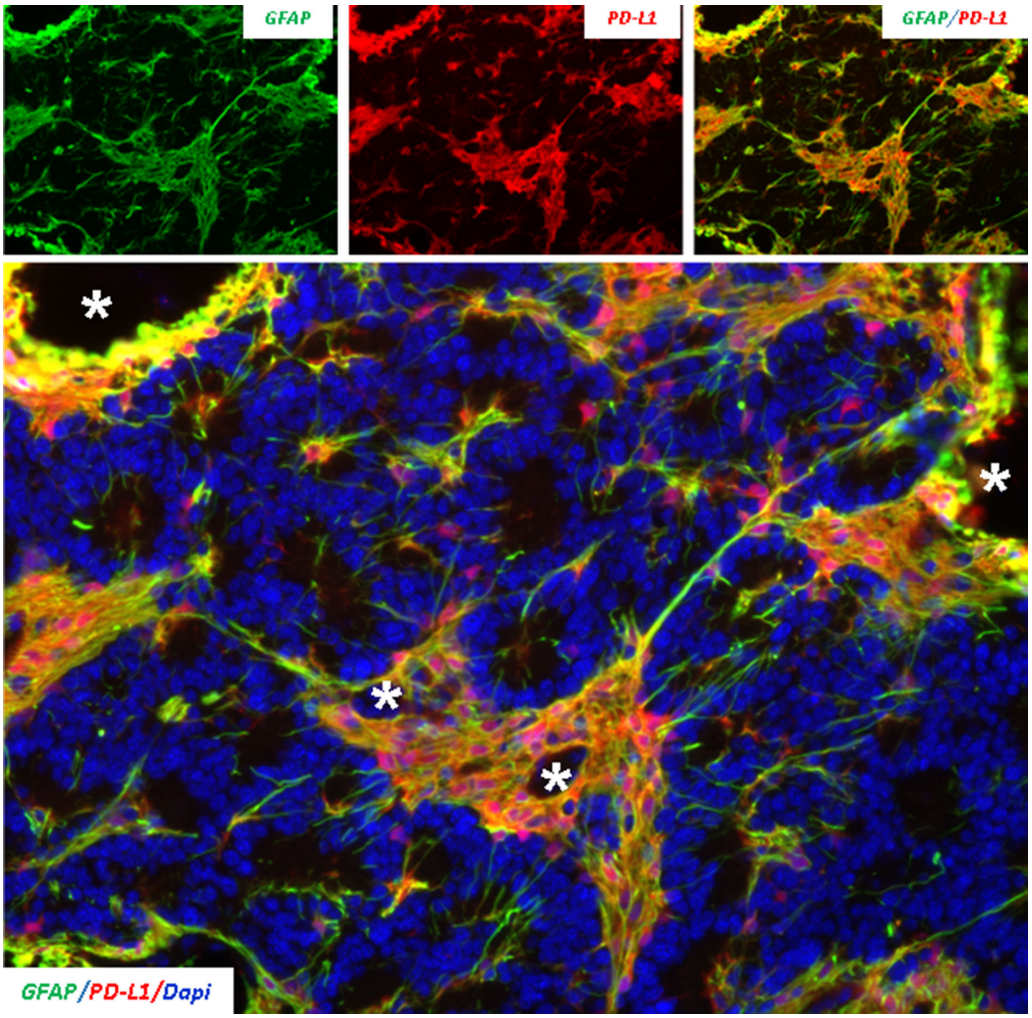

Figure 3. GFAP (*green*) and PD-L1 (*red*) double immunofluorescence in a group 1 RB not showing regression. Nuclei are stained blue with DAPI. PD-L1 positivity in perivascular glial cells (*asterisks* in the vessel lumen) and, partly, in their processes mixed with PD-L1–negative RB-viable cells. Merge images in the *box* at the *top* (GFAP and PD-L1), on the *right*, and in the *bottom box* (GFAP, PD-L1, and DAPI). Magnification × 200.

Untreated RBs Differ From CHT-Treated RBs in the Frequency of TI-Ics

In regressed RB, the frequency of almost all TI-ICs increased significantly, suggesting a complex involvement of TI-ICs. A robust response of antitumor T cells emerged, mainly supported by CD4+, CD8+, granzyme-b+, and TIA-1+ lymphocytes and macrophages, which are the main subsets responsible for the control of tumor growth. Both CD4+ and CD8+ cells can release interferon γ (IFN-γ), a main determinant of tumor regression.[40,41] We registered an increase of TIA-1+ cells that outnumbered CD8+ cells; probably partly because of an increase of TIA-1+ natural killer (NK) cells, that we did not evaluate.

CHT, besides directly killing cancer cells, triggers immunogenic cell death. Apoptosis is induced by therapy in RB.[42] However, the CHT-induced extracellular vesicles released by damaged cells can be either proimmune or immunosuppressive, depending on their content and on the TME.[43] Intriguingly, melphalan-derived vesicles can cause the release of IFNγ by NK cells.[44] This might have been a contributory mechanism to the increase in effector cells that we demonstrated in group 2 patients treated with melphalan. In our study, multiplexed immunostaining for TIA-1, CD8, and PD-1 showed that the majority of the CD8+ cells were also TIA-1+, whereas they did not express PD-1, which is an indicator of CD8 cell exhaustion.[7,45] This immune profile identifies active CD8+ lymphocytes, which likely retain their effector properties, although more investigations are mandatory to better profile their functionality.

S-100+CD1a+ dendritic-like cells were sparse in group 1 and increased significantly in chemoreduced RBs.

After CHT, we observed a significant increase in CD68+ and CD163+ macrophages as well. M1 (proinflammatory/tumoricidal) and M2 (anti-inflammatory/protumorigenic) macrophages express a functional state and can switch between phenotypes, depending on the context.[4] In humans, however, CD163 is still considered a marker of M2 macrophages, which are correlated with upregulated PD-L1 in cancer.[46] Their re-education is the aim of novel immunotherapy, and the concomitant i-CP blockade was demonstrated to yield a synergistic effect.[46]

Investigative Ophthalmology & Visual Science

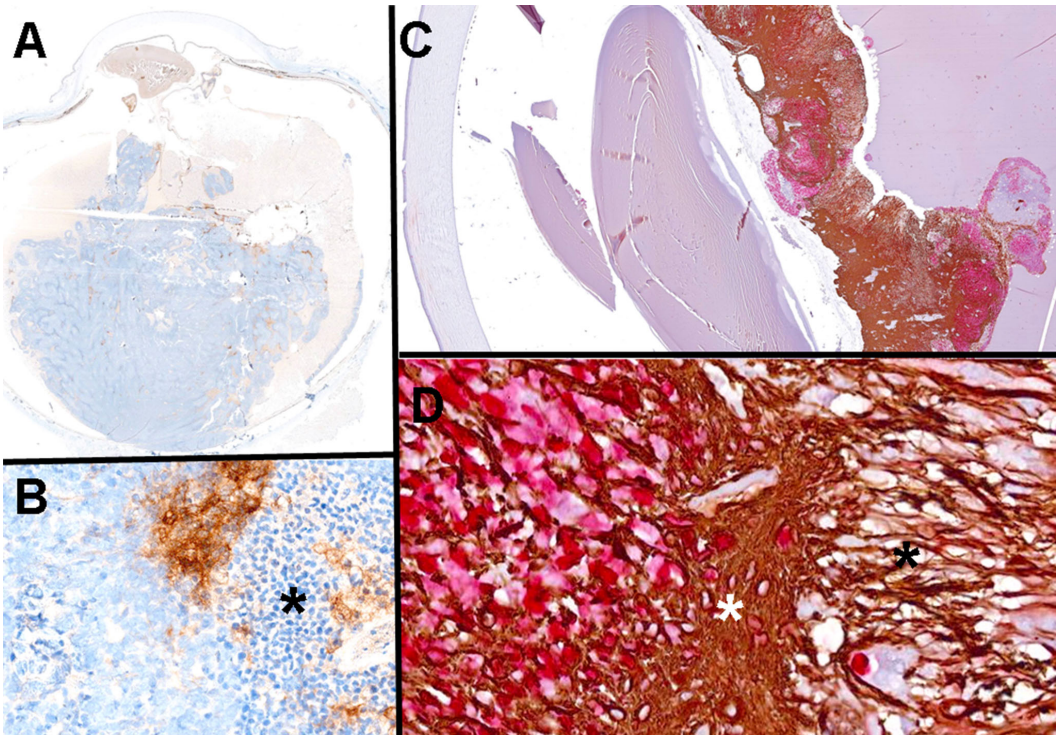

Figure 4. (**A, B**) Conventional immunohistochemistry for PD-L1: A representative case of group 1 RB, almost completely negative for PD-L1 (**A**). PD-L1 positivity is limited to few RB cells within necrotic areas (**B**, *asterisk*), and in perivascular areas. (**C, D**) Ki67 (*red*) and PD-L1 (*brown*) double immunohistochemistry in a group 3 chemoreduced RB. Note the heterogeneous frequency of Ki67+ nuclei, high in viable RB cells on the left (**D**) and very low within a PD-L1+ (*white asterisk*) gliotic area blending with a retinocytoma-like area (*black asterisk*), which also shows few Ki67+ nuclei (**D**). Magnification: **A, C**: ×1; **B**: ×200; **D**: ×400.

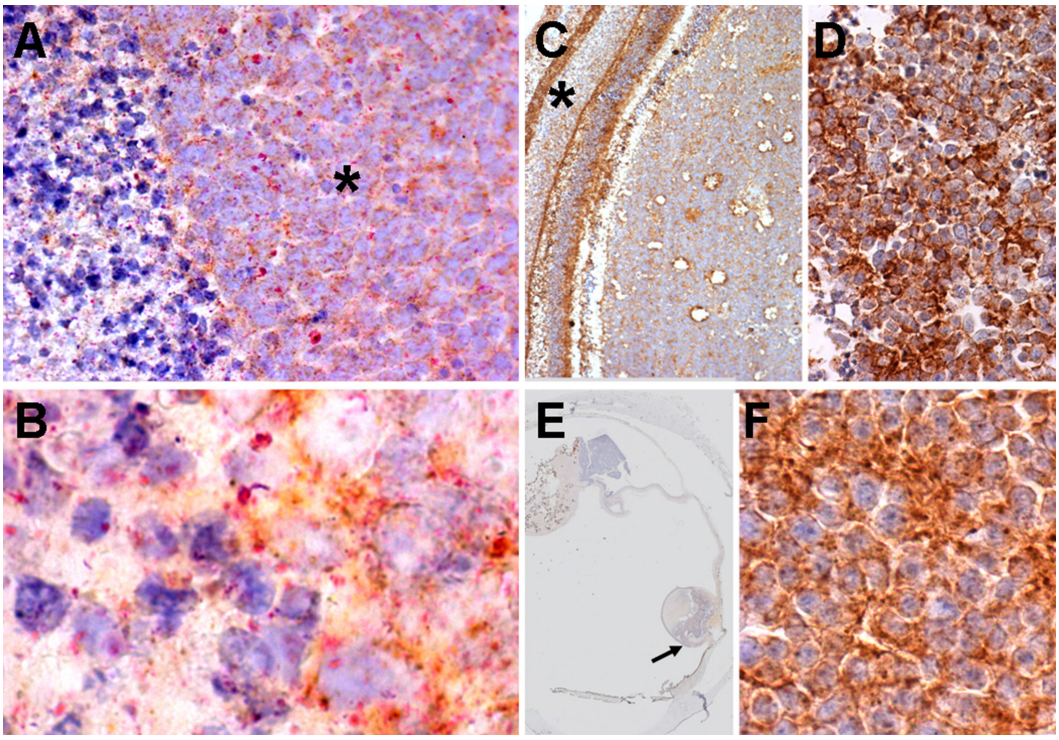

Figure 5. (**A, B**) Multiplexed immunohistochemistry for PD-1 (*brown*), CD8 (*blue*), and TIA-1 (*red*). Representative case of group 2 patients. (**A**) Inflammatory infiltrate (on the *left*) and an area of viable RB tissue (*asterisk*). (**B**) Detail showing brown-stained, PD-1+ RB cells on the right, and CD8+ blue–stained lymphocytes on the left; most CD8+ lymphocytes co-express TIA-1 (*red*, granular stain); red cytotoxic granules are also detectable admixed with RB cells. (**C, D, E, F**) Conventional immunohistochemistry for PD-1. (**C**) A group 1 RB expressing high PD-1; PD-1 positivity is also observable within the retina (*asterisk*). (**D**) Detail of PD-1 cytoplasmic positivity of RB cells. (**E**) A group 3 RB at scanning power; the *arrow* indicates an area of viable RB tissue showing PD-1 cytoplasmic positivity (**F**). Magnification: **A**: ×200; **B, D, F**: ×400; **C**: ×100; **E**: ×1. The red chromogen new fuchsin, the brown chromogen diaminobenzidine and the blue chromogen HighDef Blue were used.

Investigative Ophthalmology & Visual Science

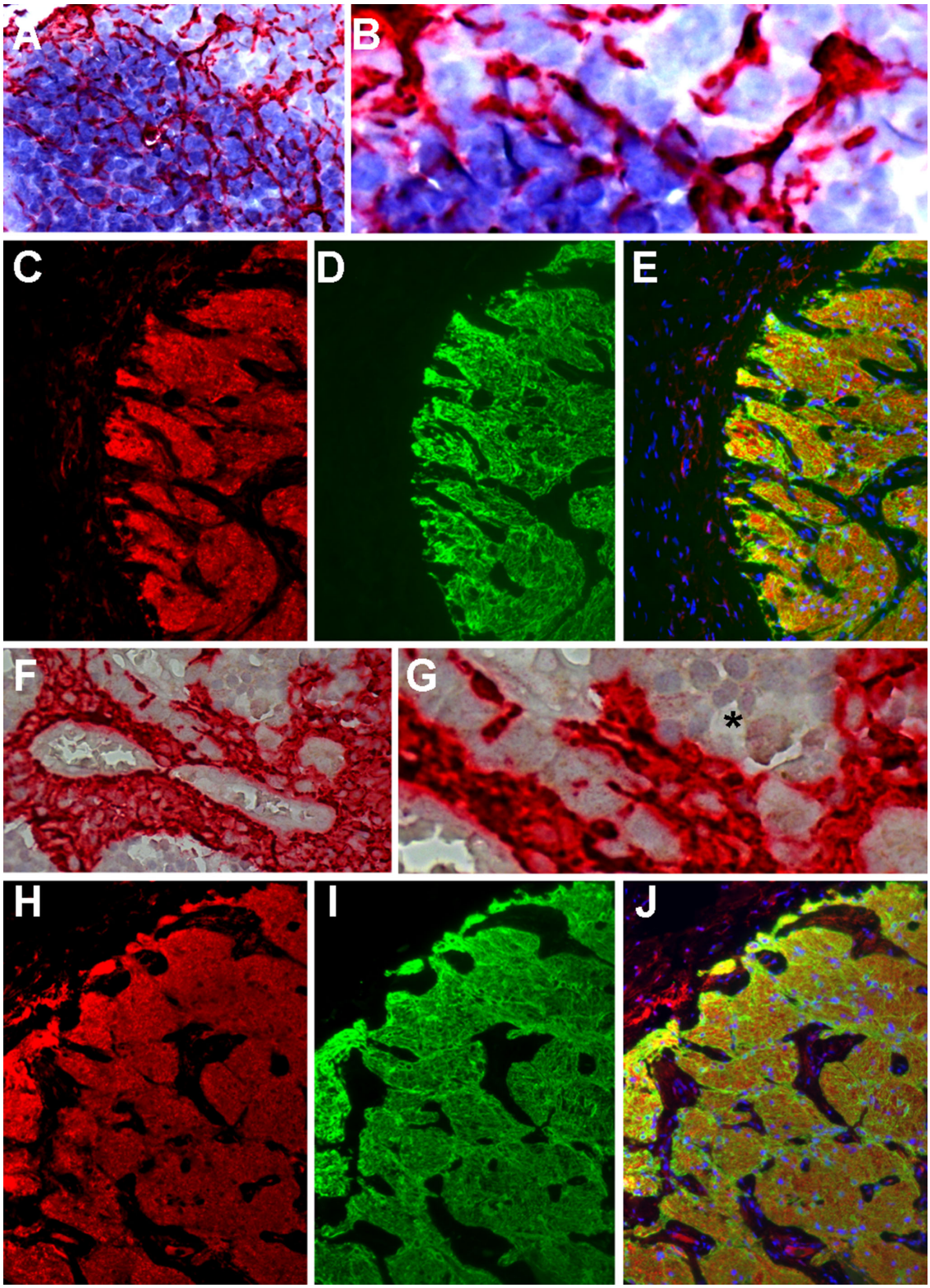

Figure 6. (**A, B, F, G**) Multiplexed immunohistochemistry for synaptophysin (*blue*); GFAP (*red*), and PD-L1 (*brown*). (**C–E, H–J**) Immunofluorescence for PD-L1 (*red*) and GFAP (*green*) (**A**) Representative case of group 2 patients; viable RB tumor cells (*blue*) identified by positivity to synaptophysin, admixed with glial cells. (**B**) Detail of glial cells coexpressing GFAP (*red*) and PD-L1 (*brown*). (**C–E**) Immunofluorescence for PD-L1 (**C**, *red*) and GFAP (**D**, *green*) in a gliotic area of another case of group 2 RB. Merge image (**E**) shows extensive colocalization of PD-L1 and GFAP and DAPI-stained RB nuclei (*blue*). (**F, G**) Multiplexed immunohistochemistry for GFAP (*red*) and PD-L1 (*brown*) in a RB of group 3. The detail (**G**) shows coexpression of GFAP and PD-L1 within a gliotic area; the *asterisk* indicates viable RB cells virtually negative to PD-L1. (**H–J**) Immunofluorescence for PD-L1 (**H**, *red*) and GFAP (**I**, *green*) in the same case. In the merge image (**J**), GFAP colocalizes with PD-L1. Magnification: **A,B, F,G**: ×400; **C–E, H–J**: ×200.

Investigative Ophthalmology & Visual Science

Table 4. Median and Range of Values for Each TME Parameter Divided by Treatment Group and Comparison Across the Three Treatment Groups (Kruskal Wallis Test: Pairwise Comparison)

	Group 1		*P* Value		Group 2		*P* Value	Group 3	
Parameters	**Median**	**Range**	**Gr 1 vs. Gr 2**	**Gr 1 vs. Gr 3**	**Median**	**Range**	**Gr 2 vs. Gr 3**	**Median**	**Range**
Age	24	2–88	<0.0001	ns	42	14–112	ns	32	4–142
CD4+	1.9	0.4–7	<0.0001	<0.0001	6.4	0.1–13	ns	6.2	0.8–12.7
CD8+	0.8	0.2–46.5	<0.0001	<0.0001	18	4.3–73.4	ns	18	14–60.1
Granzyme B+	0.1	0–3.3	<0.0001	<0.0001	1	0.2–10.6	ns	0.7	0.1–6.6
TIA-1+	0.5	0–36.2	<0.0001	<0.0001	13.2	3.5–40.4	ns	12.7	7.6–20
FOXP3+	1	0.1–2.3	ns	ns	0.7	0.1–2	ns	0.6	0.1–4.1
CD20+	0.5	0–4.7	ns	ns	0.5	0–3.7	ns	0.8	0–1.8
CD1a+/S100+	0.4	0.1–4	<0.0001	<0.0001	1.1	0.1–6	ns	1	0.3–5
CD68+	12.4	5.7–72.9	0.002	<0.0001	37	17–55	ns	38.3	8–61.7
CD163+	8.4	5–108.3	<0.0001	<0.0001	46.2	30–81.4	ns	46.2	24–105.4
CD11b+/CD14−/CD15+	2.2	0.3–12.4	0.001	ns	0.7	0.2–9.2	ns	0.8	0.1–13
Ki67+%	85	38.1–90.7	<0.0001	<0.0001	46.2	2.8–83	ns	38.8	4.8–64
GFAP+%	10.3	3.1–47.5	<0.0001	<0.0001	39.4	2.6–90.7	ns	44	21.8–86
PD-1+	1.2	0.3–20	0.04	ns	2.2	0.2–31.6	ns	2	0.7–10.7
PD-L1+%	0	0–28.3	<0.0001	<0.0001	21	0–62.1	ns	23	5–50
CD34+	5.2	0.3–12.4	ns	ns	5.1	1.9–14.6	ns	4.7	2.7–11.3

Group 1, no CHT; Group 2, IAC; Group 3, S-CHT.
ns, not significant.

Myeloid-derived suppressor cells (MDSCs), subdivided into monocytic (Mo-MDSCs, CD11b+ CD14+ CD15-) and granulocytic (G-MDSCs, CD11b+CD14-CD15+) subsets, exert multiple immunosuppressive functions.[4] Their identification by immunohistochemistry is complex.[4] The term MDSC-like is therefore recommended.[4]

We found few G-MDS-like cells in all groups; however, their frequency decreased significantly in group 2.

CHT-Does Not Affect the Frequency of FOXP3+Tregs and CD20+ Lymphocytes

Tregs, reliably identified by FOXP3 staining,[47] are crucial in the inhibition of antitumor immunity in other cancers.[4,48] They were sparse in the cold TME of group 1 RB, and did not vary in regressed RBs, however, their positive correlation with AG-M, suggests a possible role in RB as well.

The multiple functions of CD20+ lymphocytes within TME are starting to be unraveled.[49] In all our cases, their frequency was low and did not change after CHT.

CHT-Treated RBs Differ From Untreated RBs in the Extent of Gliosis, PD-1+ TI-ICs and PD-L1 Expression: RB Cells Express PD-1

In treated RBs, we observed a significantly higher gliosis than in untreated cases. Gliosis was high in five spontaneously regressed group 1 RBs as well.

In a previous study, a poor prognostic impact was associated to gliosis, because of its production of the insulin-like growth factor protein–5.[13] Recently, Singh et al.[18] reported an increased expression of PD-L1 and PD-1 in stromal/immune cells and a decreased expression of PD-L1 and an increased expression of PD-1 in RB cells after chemoreduction.[20] These factors were associated with some pathological determinants of metastatic risk and degree of anaplasia, bearing an impact on prognosis. We observed that gliotic areas strongly expressed PD-L1, which may contribute to the negative prognostic impact of gliosis.

These data indicate that PD-L1 and PD-1 may be suitable candidates for immunotherapy in RB. Recently, the expression of B7H3, another member of the B7 family, showed correlation with clinical and pathological data in RB.[19] The B7 family therefore deserves further study in RB.

The assessment of PD-L1 expression in cancer by immunohistochemistry is standardized and is the most common method to predict anti-PD-1/anti-PD-L1 therapeutic response across different cancers.[29,50–52]

PD-1 is constitutively expressed by activated T lymphocytes and macrophages and by other TI-ICs after cytokine stimuli.[53] Binding of PD-1 to PD-L1 inhibits T-cell activation, allowing immunosuppression and neoplastic growth. Blockade of this interaction has yielded therapeutic benefits in many patients.[53] In our cases, the frequency of PD-1+ TI-ICs was not very high, but it increased significantly in groups 2 and 3.

PD-L1 expression in cancer can be influenced by many intracellular and extracellular signals.[50] PD-L1 expression may be induced by IFN-γ[53]; this mechanism, documented also in a RB cell line,[38] may have occurred in group 2 patients, who received melphalan therapy, which is known to induce release of IFNγ.[44]

We did not observe colocalization of CD8 and PD-1; furthermore, CD8+ cells largely exceeded the number of PD-1 + TI-IC in all three groups.

As recently observed by Singh et al.,[20] we found RB cells expressing PD-1 to a variable extent, with a similar incidence across the three groups (20.5% cases of group 1 and 20.8% in all chemoreduced RBs).

Nowadays the targets of PD-1 inhibitors are lymphocytes and not cancer cells[54]; PD1+ tumor cells could be an interesting future therapy candidate.

CHT Turns RB TME From Cold (Immune Type II) To Hot (Immune Type I)

The composition, the functionality, and the spatial disposition of the immune infiltrate, which vary across different cancer types, identify different subclasses of TME for

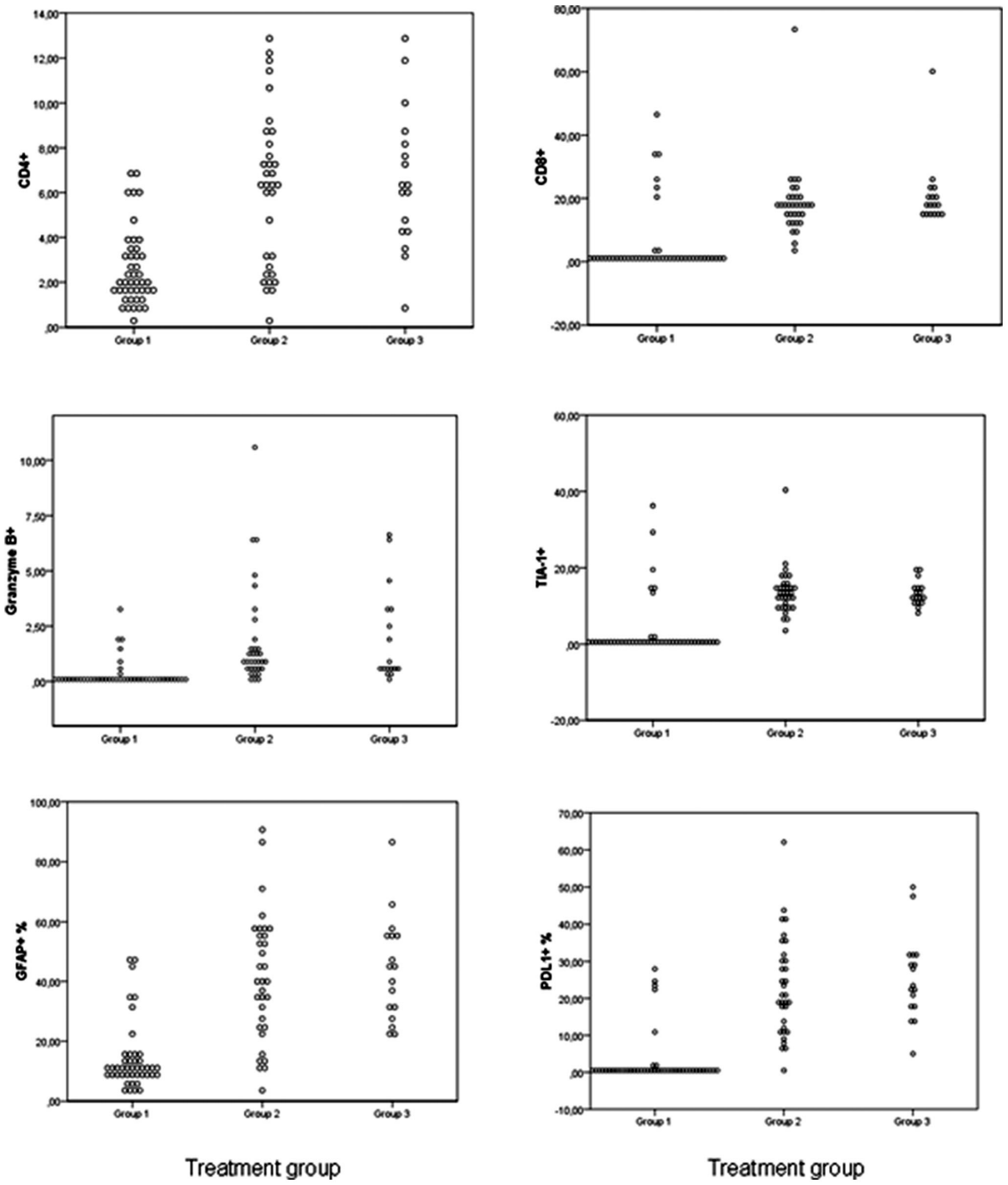

Figure 7. Distribution values of CD4+, CD8+, Granzyme B+ and TIA-1+ lymphocytes, and percentage of GFAP+ and PD-L1+ areas across the three treatment groups.

Table 5. Distribution of Histopathological Factors Across Treatment Groups

Histopathological Factors	Group 1 (n = 44)	Group 2 (n = 33)	Group 3 (n = 17)
HHRF*			
Absent	16 (36)	24 (73)	10 (58)
Present	28 (64)	9 (27)	7 (41)
Anaplasia grade*			
Retinocytoma	0 (0)	2 (6)	0 (0)
Mild	16 (36)	24 (73)	11 (65)
Moderate	23 (52)	7 (21)	6 (35)
Severe	5 (11)	0 (0)	0 (0)

* Number (percentage)

Investigative Ophthalmology & Visual Science

Table 6. Correlation Between TME Parameters and Histopathological Features

	HHRF		AG-M	
Parameters	**Coeff***	***P* Value**	**Coeff***	***P* Value**
CD4+	−0.174	0.09	−0.235	0.02
CD8+	−0.229	0.03	−0.495	<0.001
Granzyme B+	−0.221	0.04	−0.446	<0.001
TIA-1+	−0.222	0.03	−0.452	<0.001
FOXP3+	0.005	0.96	0.376	<0.001
CD20+	0.079	0.45	0.176	0.09
CD1a+/S100+	−0.067	0.52	−0.409	<0.001
CD68+	−0.173	0.1	−0.398	<0.001
CD163+	−0.134	0.2	−0.453	<0.001
CD11b+/CD14-/CD15+	0.274	0.007	0.230	0.03
Ki67+%	0.296	0.004	0.597	<0.001
GFAP+%	−0.272	0.008	−0.494	<0.001
PD-1+	−0.051	0.625	−0.229	0.03
PD-L1+%	−0.259	0.01	−0.507	<0.001
CD34+	−0.006	0.95	−0.029	0.78

* Spearman's rho correlation coefficient.

treatment planning and prediction of response to immunotherapy.[4,55] Based on the CD8+ cytotoxic T-cell status and the expression of PD-L1, some authors subclassified cancer into four different immune types.[6,56] A CD8+ and PD-L1+ TME scenario has been defined as immune type I, whereas the coexistence of virtually absent or functionally excluded TI-ICs with PD-L1 immunonegativity characterized the immune type II cancer TME.[6,56]

In Group 1, the majority of cases ($n = 39$ [88.6%]) showed a cold TME (CD8−; PD-L1−), which was positively correlated with the presence of HHRFs and high AG-M.

Conversely, 49 of 50 (98%) chemoreduced RBs showed an active immune signature (high CD8+; TIA-1+; PD-L1+), which was negatively correlated with the presence of HHRFs and a high AG-M.

In our experience, RB regression, either spontaneous or induced by CHT, was accompanied by a reprogrammed RB TME, from type II (cold) to type I (hot), suggesting a novel immunotherapeutic scenario. Immunotherapy combined with CHT could allow less-intensive treatment regimens. Epigenetic promoter hypermethylation occurs in RB,[57] as observed also by us.[58] Moreover, the combination of hypomethylating and immunomodulatory agents is yielding promising results in cancer, as we observed in unresectable melanoma.[27]

Conclusions

The perspective of modulating the immune response in RB for therapeutic purposes is interesting. Immunotherapy requires knowledge of the TME components, their multifaceted functions and spatial distribution, for which multiplexed analyses at tumor tissue level are very informative. In our experience, all regressed RBs showed TME changes in a similar manner; correlative studies between next-generation imaging and TME could better profile cohorts of patients for novel treatments.

Acknowledgments

The authors thank Marzio Vestri for his technical support. We also acknowledge the contributions of ASROO, scientific society of Retinoblastoma and Ocular Oncology.

Supported by Liberal Grant and Institutional Funding; PAR 2018, University of Siena.

Disclosure: **C. Miracco,** None; **P. Toti,** None; **M. Chiara Gelmi,** None; **S. Aversa,** None; **G. Baldino,** None; **P. Galluzzi,** None; **S. De Francesco,** None; **F. Petrelli,** None; **E. Sorrentino,** None; **G. Belmonte,** None; **D. Galimberti,** None; **S. Bracco,** None; **T. Hadjistilianou,** None

References

1. PDQ Pediatric Treatment Editorial Board Retinoblastoma Treatment (PDQ): Health Professional Version. In: *PDQ Cancer Information Summaries*. Bethesda, MD: National Cancer Institute (US); 2019.
2. Global Retinoblastoma Study Group. Global Retinoblastoma Presentation and Analysis by National Income Level. *JAMA Oncol*. 2020;6(5):685–695.
3. Andersch L, Radke J, Klaus A, et al. CD171- and GD2-specific CAR-T cells potently target retinoblastoma cells in preclinical in vitro testing. *BMC Cancer*. 2019;19(1):895.
4. Thorsson V, Gibbs DL, Brown SD, et al. The immune landscape of cancer. *Immunity*. 2019;51(2):411–412.
5. Zemek RM, De Jong E, Chin WL, et al. Sensitization to immune checkpoint blockade through activation of a STAT1/NK axis in the tumor microenvironment. *Sci Transl Med*. 2019;11(501):eaav7816.
6. Teng MW, Ngiow SF, Ribas A, Smyth MJ. Classifying cancers based on T-cell infiltration and PD-L1. *Cancer Res*. 2015;75(11):2139–2145.
7. Hendry S, Salgado R, Gevaert T, et al. Assessing tumor-infiltrating lymphocytes in solid tumors: a practical review for pathologists and proposal for a standardized method from the International Immunooncology Biomarkers Working Group: Part 1: Assessing the host immune response, TILs in Invasive Breast Carcinoma and Ductal Carcinoma In Situ, Metastatic Tumor Deposits and Areas for Further Research. *Adv Anat Pathol*. 2017;24(5):235–251.
8. Madigan MC, Penfold PL. Human retinoblastoma: a morphological study of apoptotic, leukocytic, and vascular elements. *Ultrastruct Pathol*. 1997;21(2):95–107.
9. Alegret AM, Jockovich M, Pina Y, Boutrid H, Hernandez E, Murray T. Tumor infiltrating lymphocytes in retinal tumors from LHBETATAG mice. *Invest Ophthalmol Vis Sci*. 2008;49(13):75.
10. Murray TG, Cebulla CM, Alegret A, Pina Y, Boutrid Jockovich ME. Targeting the tumor TME as a therapeutic strategy for retinoblastoma. *Invest Ophthalmol Vis Sci*. 2007;48:1585–1585.
11. Boutrid H, Piña Y, Cebulla CM, et al. Increased hypoxia following vessel targeting in a murine model of retinoblastoma. *Invest Ophthalmol Vis Sci*. 2009;50(12):5537–5543.
12. Piña Y, Boutrid H, Murray TG, et al. Impact of tumor-associated macrophages in LH(BETA)T(AG) mice on retinal tumor progression: relation to macrophage subtype. *Invest Ophthalmol Vis Sci*. 2010;51(5):2671–2677.
13. Xu XL, Lee TC, Offor N, et al. Tumor-associated retinal astrocytes promote retinoblastoma cell proliferation through production of IGFBP-5. *Am J Pathol*. 2010;177(1):424–435.
14. Bond WS, Akinfenwa PY, Perlaky L, Hurwitz MY, Hurwitz RL, Chevez-Barrios P. Tumorspheres but not adherent cells derived from retinoblastoma tumors are of malignant origin. *PLoS One* 2013;8:e63519.
15. Sudhakar J, Venkatesan N, Lakshmanan S, Khetan V, Krishnakumar S,, Biswas J. Hypoxic tumor microenvironment in advanced retinoblastoma. *Pediatr Blood Cancer*. 2013;60:1598–1601.

16. Raguraman R, Parameswaran S, Kanwar JR, et al. Evidence of tumour TME and stromal cellular components in retinoblastoma. *Ocul Oncol Pathol* 2019;5:85–93.
17. Singh L, Kashyap S, Pushker N, Bakhshi S, Sen S, Rizvi MA. Expression pattern of immune checkpoints programmed death (PD-1) and programmed death-ligand (PD-L1) in retinoblastoma and its prognostic significance. *Ann Oncol*. 2017;28(suppl_11):xi6–xi29.
18. Singh L, Singh MK, Rizvi MA, Kashyap S. Interaction of immune checkpoints in tumor-stromal TME of primary and chemoreduced retinoblastoma. *Invest Ophthalmol Vis Sci*. 2019;60 (9):2319.
19. Ganesan B, Parameswaran S, Sharma A, Krishnakumar S. Clinical relevance of B7H3 expression in retinoblastoma. *Sci Rep* 2020;10(1):10185.
20. Singh L, Singh MK, Rizvi MA, et al. Clinical relevance of the comparative expression of immune checkpoint markers with the clinicopathological findings in patients with primary and chemoreduced retinoblastoma. *Cancer Immunol Immunother*. 2020;69(6):1087–1099.
21. Parra ER, Francisco-Cruz A, Wistuba II. State-of-the-art of profiling immune contexture in the era of multiplexed staining and digital analysis to study paraffin tumor tissues. *Cancers (Basel)*. 2019;11(2):247.
22. Sastre X, Chantada GL, Doz F, et al. International Retinoblastoma Staging Working Group: proceedings of the consensus meetings from the International Retinoblastoma Staging Working Group on the pathology guidelines for the examination of enucleated eyes and evaluation of prognostic risk factors in retinoblastoma. *Arch Pathol Lab Med*. 2009; 133 (8): 1199–1202.
23. Mendoza PR, Specht CS, Hubbard GB, et al. Histopathologic grading of anaplasia in retinoblastoma. *Am J Ophthalmol*. 2015; 159:764–776.
24. Guasti A, Leonini S, Bertelli E, et al. Intra-arterial chemotherapy for retinoblastoma: the dosimetric impact. *Neuroradiology*. 2019;61(9):1083–1091.
25. Mallipatna A, Gallie BL, Chévez-Barrios P. Retinoblastoma. In: Amin MB, Edge SB, Greene FL, eds. *AJCC Cancer Staging Manual*, 8th ed. New York: Springer; 2017; 819–831.
26. Danielli R, Patuzzo R, Di Giacomo AM, et al. Intralesional administration of L19-IL2/L19-TNF in stage III or stage IVM1a melanoma patients: results of a phase II study. *Cancer Immunol Immunother*. 2015;64(8):999–1009.
27. Di Giacomo AM, Covre A, Finotello F, et al. Guadecitabine plus ipilimumab in unresectable melanoma: The NIBIT-M4 Clinical Trial. *Clin Cancer Res*. 2019;25(24):7351–7362.
28. Pecorelli A, Natrella F, Belmonte G, et al. NADPH oxidase activation and 4-hydroxy-2-nonenal/aquaporin-4 adducts as possible new players in oxidative neuronal damage presents in drug-resistant epilepsy. *Biochim Biophys Acta*. 2015;1852(3):507–519.
29. O'Malley DP, Yang Y, Boisot S, et al. Immunohistochemical detection of PD-L1 among diverse human neoplasms in a reference laboratory: observations based upon 62,896 cases. *Mod Pathol*. 2019;32(7):929–942.
30. Ghassemi F, Rahmanikhah E, Roohipoor R, Karkhaneh R, Faegh A. Regression patterns in treated retinoblastoma with chemotherapy plus focal adjuvant therapy. *Pediatr Blood Cancer*. 2013;60:599–604.
31. Bechrakis NE, Bornfeld N, Schueler A, Coupland SE, Henze G, Foerster MH. Clinicopathologic features of retinoblastoma after primary chemoreduction. *Arch Ophthalmol*. 1998;116(7):887–893.
32. Dithmar S, Aabert TM, Grossniklaus HE. Histopathologic changes in retinoblastoma after chemoreduction. *Retina*. 2000;20(1):33–36.
33. Demirci H, Eagle RC, Shields CL, Shields JA. Histopathologic findings in eyes with retinoblastoma treated only with chemoreduction. *Arch Ophthalmol*. 2003;121(8):1125–1131.
34. Shields CL, Palamar M, Sharma P, et al. Retinoblastoma regression patterns following chemoreduction and adjuvant therapy in 557 tumors. *Arch Ophthalmol*. 2009;127(3):282–290.
35. Graeber CP, Gobin YP, Marr BP, et al. Histopathologic findings of eyes enucleated after treatment with chemosurgery for retinoblastoma. *Open Ophthalmol J*. 2011;5:1–5.
36. Alsharif H, Helmi H, Maktabi A. Histopathological characteristics and classification for prognostic indicators. In: Alkatan HM, ed. *Retinoblastoma—Past, Present and Future*. London: IntechOpen. 2019:89–99.
37. Damodaran S, Bajaj MS, Sharma P, et al. Swept-source optical coherence tomography features of regressed macular retinoblastoma. *Ind J Ophthalmol*. 2019;67:2013–2018.
38. Usui Y, Okunuki Y, Hattori T, et al. Expression of costimulatory molecules on human retinoblastoma cells Y-79: Functional expression of CD40 and B7H1. *Invest Ophtalmol Vis Sci*. 2006;47:4607–4613.
39. Goodman AM, Kato S, Bazhenova L, et al. Tumor mutational burden as an independent predictor of response to immunotherapy in diverse cancers. *Mol Cancer Ther*. 2017;16(11):2598–2608.
40. Ostroumov D, Fekete-Drimusz N, Saborowski M, Kühnel F, Woller N. CD4 and CD8 T lymphocyte interplay in controlling tumor growth. *Cell Mol Life Sci*. 2018;75(4):689–713.
41. Rosenberg J, Huang J. $CD8^+$ T Cells and NK cells: parallel and complementary soldiers of immunotherapy. *Curr Opin Chem Eng*. 2018;19:9–20.
42. Jockovich ME, Suarez F, Alegret A, et al. Mechanism of retinoblastoma tumor cell death after focal chemotherapy, radiation, and vascular targeting therapy in a mouse model. *Invest Ophthamol Vis Sci*. 2008;48(12):5371–6.
43. Ab Razak NS, Ab Mutalib NS, Mohtar MA, Abu N. Impact of chemotherapy on extracellular vesicles: understanding the chemo-EVs. *Front Oncol*. 2019;9:1113.
44. Vulpis E, Cecere F, Molfetta R, et al. Genotoxic stress modulates the release of exosomes from multiple myeloma cells capable of activating NK cell cytokine production: Role of HSP70/TLR2/NF-kB axis. *Oncoimmunology*. 2017;6(3):e1279372.
45. Berger KN, Pu JJ. PD-1 pathway and its clinical application: a 20year journey after discovery of the complete human PD-1 gene. *Gene*. 2018;638:20–5.
46. Kowal J, Kornete M, Joyce JA. Re-education of macrophages as a therapeutic strategy in cancer. *Immunotherapy*. 2019;11(8):677–689.
47. Georgiev P, Charbonnier LM, Chatila T. Regulatory T Cells: the Many Faces of Foxp3. *J Clin Immunol*. 2019;39(7):623–640.
48. Miracco C, Mourmouras V, Biagioli M, et al. Utility of tumour-infiltrating CD25+FOXP3+ regulatory T cell evaluation in predicting local recurrence in vertical growth phase cutaneous melanoma. *Oncol Rep*. 2007;18(5):1115–1122.
49. Guo FF, Cui JW. The role of tumor-infiltrating B cells in tumor immunity. *J Oncol*. 2019;2019:2592419.
50. Wu Y, Chen W, Xu ZP, Gu W. PD-L1 Distribution and perspective for cancer immunotherapy-blockade, knockdown, or inhibition. *Front Immunol*. 2019;10:2022.
51. Yi M., Jiao D., Xu H., et al.. Biomarkers for predicting efficacy of PD-1/PD-L1 inhibitors. *Mol Cancer*. 2019;17: 129.
52. Rimm DL, Han G, Taube JM, et al. A prospective, multi-institutional, pathologist-based assessment of 4 immunohistochemistry assays for PD-L1 expression in non-small cell lung cancer. *JAMA Oncol*. 2017;3(8):1051–1058.

Investigative Ophthalmology & Visual Science

53. Qin W, Hu L, Zhang X, et al. The diverse function of PD-1/PD-L pathway beyond cancer. *Front Immunol*. 2019;10:2298.
54. Shang YH, Zhang Y, Li JH, Li P, Zhang X. Risk of endocrine adverse events in cancer patients treated with PD-1 inhibitors: a systematic review and meta-analysis. *Immunotherapy*. 2017;9(3):261–272.
55. Duan Q, Zhang H, Zheng J, Zhang L. Turning cold into hot: firing up the tumor microenvironment. *Trends Cancer*. 2020;6(7):605–618.
56. Ock CY, Keam B, Kim S, et al. Pan-cancer immunogenomic perspective on the tumor microenvironment based on PD-L1 and CD8 T-cell infiltration. *Clin Cancer Res*. 2016;22(9):2261–2270.
57. Zhang J, Benavente CA, McEvoy J, et al. A novel retinoblastoma therapy from genomic and epigenetic analyses. *Nature*. 2012;481(7381):329–334.
58. Gelli E, Pinto AM, Somma S, et al. Evidence of predisposing epimutation in retinoblastoma. *Hum Mutat*. 2019;40(2):201–206.